Applied Physics B (2019) 125:54
https://doi.org/10.1007/s00340-019-7138-7

Applied Physics B
Lasers and Optics

Ultrahigh-contrast cross-polarized entangled photon pairs from a strongly birefringent photonic-crystal fiber

N. L. Petrov[1] · A. A. Voronin[1,3,4] · A. B. Fedotov[1,3,4] · A. M. Zheltikov[1,2,3,4,5]

Received: 15 February 2018 / Accepted: 16 January 2019 / Published online: 4 March 2019

Abstract
Four-wave mixing with cross-polarized pump and cross-polarized sidebands is identified as a powerful resource of quantum entanglement, enabling creation of efficient fiber-optic sources of entangled photon pairs. Generation of cross-polarized photon pairs is demonstrated by coupling the laser pump into orthogonal polarization modes of a highly birefringent, highly nonlinear, anomalously dispersive photonic-crystal fiber. With the pump wavelength set to lie deeply within the anomalous dispersion region of the fiber, the frequency offset of the photon pairs relative to the pump exceeds 45 THz, enhancing the contrast of photon pairs against the Raman noise to yield photon pairs with a coincidence-to-accidental ratio as high as 250: 1.

Four-wave mixing (FWM) in optical fibers offers attractive solutions for the fiber-format generation of entangled photon states [1–4]. Rapidly progressing fiber technologies provide powerful means to tailor the key parameters of optical fibers, including fiber dispersion, nonlinearity, and birefringence, opening the routes toward enhanced photon entanglement and factorable photon states [5–7]. Photonic crystal fibers (PCFs) [8] are of special interest in this regard as they promise a unique fiber-optic platform for quantum technologies, allowing tunable photon-pair generation within a broad range of pump wavelengths [1–5, 9].

Due to its vectorial nature, FWM lends a vast parameter space for tailored photon-pair generation [4, 10–16]. Vectorial FWM arrangements where two copolarized pump fields with the same frequency ω_p give rise to signal and idler sidebands at ω_s and ω_i, both generated in the polarization mode orthogonal to the polarization mode of the pump (Fig. 1a), have been shown [13–17] to help enhance the contrast of correlated photon pairs relative to the spontaneous Raman noise and to enable polarization entanglement of photon states. While the key advantages provided by this scheme of vectorial FWM for fiber-optic quantum technologies have been studied in great detail in earlier experiments [13–16], analysis of an alternative version of vectorial FWM, where two cross-polarized pump fields generate cross-polarized FWM sidebands (Fig. 1b), remains largely limited to theoretical studies [e.g., Ref. 17].

Results of experiments presented below in this paper show that this version of vectorial FWM provides a powerful resource for quantum entanglement. Unlike the FWM process shown in Fig. 1a, which is controlled by the $\chi^{(3)}_{1122}(\omega_s; -\omega_i, \omega_p, \omega_p)$-type components of the cubic susceptibility tensor, the FWM polarization arrangement of Fig. 1b connects to another type of components of this tensor—$\chi^{(3)}_{1212}(\omega_s; -\omega_i, \omega_p, \omega_p)$. Remarkably, while the two $\chi^{(3)}_{ijkl}$ components should be equal to each other in an isotropic medium off one- and multiphoton resonances, the phase-matching conditions for the two polarization arrangements of FWM, as we will show below in this paper, are different, leading to a different dependence of the photon-pair frequencies on the fiber dispersion and birefringence. Our experiments demonstrate that high-quality cross-polarized photon pairs can be generated in this FWM geometry by coupling the laser pump into orthogonal polarization modes of a highly birefringent, highly nonlinear, anomalously dispersive PCF. With the pump wavelength chosen deeply within

✉ A. M. Zheltikov
zheltikov@physics.msu.ru

[1] Physics Department, International Laser Center, M.V. Lomonosov Moscow State University, 119992 Moscow, Russia

[2] Department of Physics and Astronomy, Texas A&M University, College Station, TX 77843, USA

[3] Russian Quantum Center, ul. Novaya 100, Skolkovo, Moscow Region 143025, Russia

[4] Kazan Quantum Center, A.N. Tupolev Kazan National Research Technical University, Kazan 420126, Russia

[5] Moscow Institute of Physics and Technology, Dolgoprudny, Moscow Region 141701, Russia

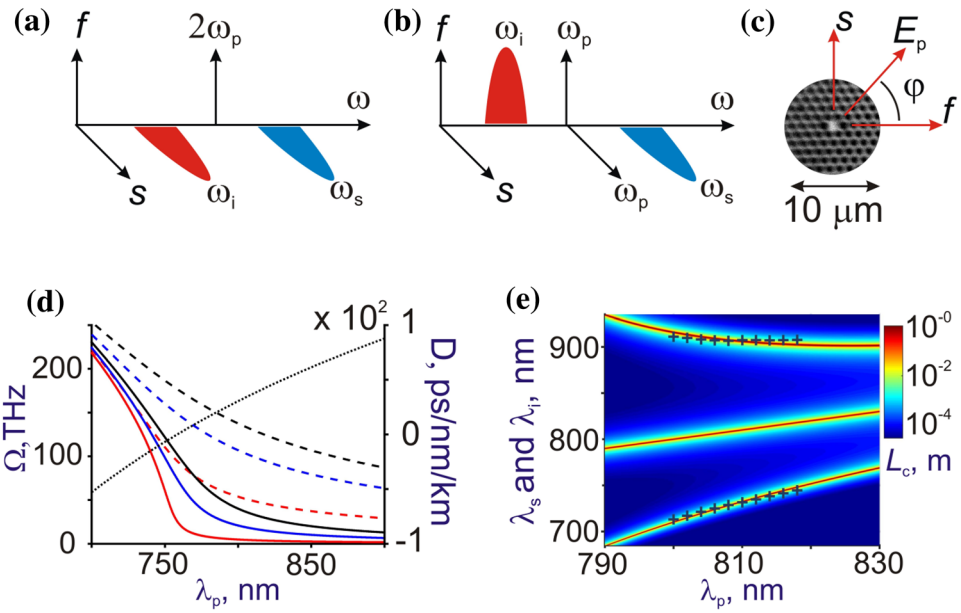

Fig. 1 **a, b** Two polarization arrangements of vectorial FWM $2\omega_p = \omega_s + \omega_i$, where two pump fields with the same frequency ω_p give rise to signal and idler sidebands at ω_s and ω_i: **a** two copolarized pump fields in the fast mode f of PCF generate signal and idler sidebands both produced in the slow mode s and **b** two cross-polarized pump fields generate signal photons in the slow mode and idler photons in the fast mode. **c** The cross section of PCF used in our experiments. **d, e** The sideband frequency shift Ω as a function of the pump wavelength calculated by numerically solving the phase-matching equation $\Delta\beta = 0$ for the $\chi^{(3)}_{1212}$ FWM (solid lines) and $\chi^{(3)}_{1122}$ FWM (dashed lines) for a dispersion profile of the PCF used in our experiments (dotted line) with birefringence $\delta n = 10^{-4}$ (red), 5×10^{-4} (blue), and 10^{-3} (black). **d** The coherence length $L_c = \pi/|\Delta\beta|$ for the $2\omega_p = \omega_s + \omega_i$ $\chi^{(3)}_{1212}$ FWM process as a function of the signal and idler wavelengths for the PCF used in our experiments with a peak pump power of 35 W. The crosses show the wavelengths of the signal and idler photons measured as a function of pump wavelength

the anomalous dispersion region of the fiber, the frequency offset of the photon pairs relative to the pump frequency is adjusted to exceed 45 THz for an efficient spectral suppression of the Raman noise, yielding photon pairs with the coincidence-to-accidental ratio (C/A) as high as 250: 1.

We start with the analysis of general properties of the $2\omega_p = \omega_s + \omega_i$ FWM process, in which two cross-polarized pump fields with the frequency ω_p give rise to signal and idler sidebands at frequencies $\omega_{s,i} = \omega_p \pm \Omega$ generated in the orthogonal, fast (f) and slow (s) polarization modes of a fiber (Fig. 1b). The phase mismatch for such a process is $\Delta\beta = \beta_s + \beta_i - \beta_p^s - \beta_p^f$, where β_p^s and β_p^f are the propagation constants of the two pump fields in the slow and fast polarization modes and β_s and β_i are the propagation constants of the signal and idler fields, respectively. If the pump peak power is low, so that the Kerr-effect nonlinear phase shifts are negligible, the propagation constants of the FWM sidebands can be approximated, within a standard approach [15–18], as $\beta_{s,i} = \beta_p^{s,f} \pm \Omega/u + \beta_2\Omega^2/2$, where u is the group velocity, and $\beta_2 = \partial^2\beta/\partial\omega^2|_{\omega_p}$ is the group-velocity dispersion (GVD) coefficient at the pump frequency, which is assumed to be the same for both polarization modes.

The phase-matching condition $\Delta\beta = 0$then dictates $\delta n\Omega/c + \beta_2\Omega^2 \approx 0$, where $\delta n = (\beta_p^s - \beta_p^f)c/\omega_p$ is the fiber birefringence. With δn and β_2 of opposite signs, this equation gives $\Omega \approx |\delta n|/(c|\beta_2|)$. The phase-matching equation for the $\chi^{(3)}_{1212}$ FWM process is strikingly different from the phase-matching equation for the $\chi^{(3)}_{1122}$ FWM process, studied in the earlier work [13–16]. When written in the same approximation, the phase-matching condition for the latter process gives $\delta n\omega_p/c + \beta_2\Omega^2 \approx 0$. Unlike the $\chi^{(3)}_{1122}$ FWM, where the sideband shift Ω scales as $(\omega_p/c)^{1/2}|\delta n/\beta_2|^{1/2}$, the sideband frequency shift in the $\chi^{(3)}_{1212}$ FWM, examined in this work, is a linear function of $|\delta n/\beta_2|$. In Fig. 1d, we compare numerical solutions of the $\Delta\beta = 0$ equation for the $\chi^{(3)}_{1212}$ and $\chi^{(3)}_{1122}$ FWM processes with a dispersion profile of the PCF used in our experiments (shown by the dotted line in Fig. 1d). This comparison shows that the photon pairs generated through the $\chi^{(3)}_{1212}$ FWM process belong to a radically different dispersion branch, helping reach new areas of the $(\Omega, \beta_2, \delta n)$ parameter space and, hence, photon-pair properties inaccessible to the photon pairs produced by the $\chi^{(3)}_{1122}$ FWM. As a general tendency, smaller fiber cores provide a stronger birefringence of orthogonal polarization modes [19], thus helping finely

tune the phase matching (Fig. 1d) for the desired pump wavelength.

In experiments, a mode-locked Ti: sapphire laser, used as a source of pump photons, is adjusted to deliver transform-limited near-infrared pulses with a central wavelength $\lambda_p \approx$ 800 nm and an FWHM pulse width of about 50 fs at a pulse repetition rate $f_p \approx 92$ MHz. To reduce the bandwidth of the pump pulses, we let the Ti: sapphire laser output pass through a spectral-narrowing unit (Fig. 2), consisting of a diffraction grating, a cylindrical lens, a slit, and a mirror, thus yielding pulses with an FWHM pulse width of about 300 fs behind a Faraday isolator. These pulses served as a pump in our experiments.

Experiments were performed with a 40-cm stretch of fused silica PCF with a slightly elliptical core with a semi-major-axis diameter $S \approx 1.8$ μm, numerical aperture NA ≈ 0.38, nonlinearity coefficient $\gamma \approx 0.10\ \mathrm{W^{-1}m^{-1}}$, and zero-GVD wavelength $\lambda_z \approx 750$ nm. The birefringence estimated from spectral fringes for this fiber is $\delta n \approx 10^{-3}$.

When launched into the fiber, a linearly polarized laser field $\boldsymbol{E}_p$ that makes an angle φ with the fast axis of the fiber (Fig. 1c) couples into fast and slow modes of the fiber with amplitudes $E_p^f = E_p cos\varphi$ and $E_p^s = E_p \sin\varphi$, which serve as pump fields in the vectorial $\chi^{(3)}_{1212}$ FWM (Fig. 1b). The field amplitudes in these modes are adjusted by rotating a half-wave plate placed in front of the input end of the fiber (Fig. 2). With the fiber dispersion profile as shown in Fig. 1d, the central wavelength of the pump field in our experiments falls deeply within the anomalous dispersion region of the fiber. In this regime, the phase matching for the $\chi^{(3)}_{1212}$ FWM process (Fig. 1d, e) dictates large Ω values. Specifically, for the peak pump power $P = 35$ W, which corresponds to an average pump power $p \sim 1$ mW, FWM sideband generation in our PCF is phase matched at Ω ≈ 45 THz (Fig. 1d). Such a large frequency shift allows correlated pairs generated through the $\chi^{(3)}_{1212}$ FWM process to be efficiently separated from uncorrelated photon pairs produced due to the spontaneous Raman effect [17, 20].

For the spectral analysis of the PCF output, a flip mirror was set to reflect the PCF output to a monochromator (Fig. 2). The photon count rate was then measured as a function of the wavelength with monochromator gratings rotated with a computer-driven stepper motor. A notch filter installed in front of the flip mirror (Fig. 2) provided an attenuation of the pump power by a factor of at least 10^{12}. The spectra measured at the PCF output (Fig. 3a) display well-resolved peaks centered at the frequencies of FWM sidebands ($\lambda_s \approx 713$ nm and $\lambda_i \approx 912$ nm for $\lambda_p \approx 800$ nm in Fig. 3a). When measured as function of λ_p, the signal and idler wavelengths λ_s and λ_i (crosses in Fig. 2e) agree well with the predictions of our phase-matching analysis. PCF output spectra also exhibit a broad feature centered roughly at ≈ 13 THz (Fig. 3a), corresponding to the peak of the Raman gain in silica fibers. Near the maximum of this peak, the photon count rate, as is readily seen from Fig. 3a, is more than two orders of magnitude higher than the signal and idler photon count rates, masking correlated FWM photon pairs with low Ω.

For photon-pair correlation studies, the signal and idler sidebands were separated from the pump with two notch filters installed in front of the dichroic mirror separating the signal and idler fields (Fig. 2). Uncorrelated photon pairs produced due to spontaneous Raman scattering were filtered from correlated photons, originating from FWM, with the short- and longpass filters with cutoff wavelengths of ≈ 750 and 900 nm, installed in the signal and idler channels, respectively. Polarization of the signal and idler

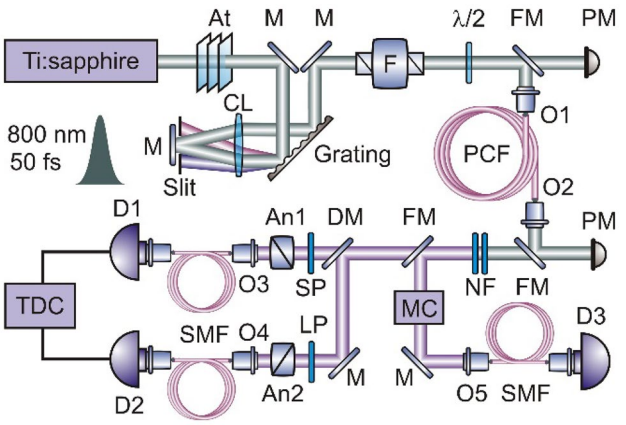

Fig. 2 Experimental setup: *M*, mirrors; *FM*, flip mirrors; *CL*, cylindrical lens; *At*, attenuators; *An1, An2*, Glan–Taylor-prism polarization analyzers; *O1–O5*, objectives; *MC*, monochromator; *PCF*, photonic-crystal fiber; *SP*, shortpass filter; *LP*, longpass filter; *SMF*, single-mode fibers; *F*, Faraday isolator; *DM*, dichroic mirror, cutoff wavelength 800 nm; *NF*, notch filter; *λ/2*, half-wave plate; *D1, D2, D3*, silicon single-photon avalanche detectors; *TDC*, time-to-digital converter for time-correlated single-photon counting

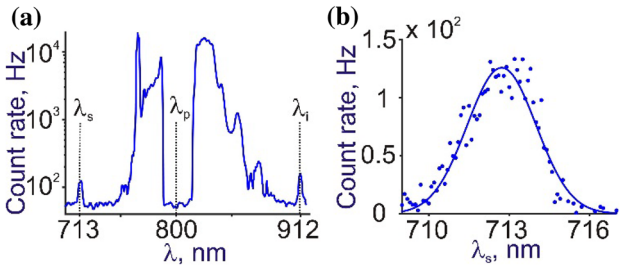

Fig. 3 **a** The spectrum of the PCF output and **b** the count rate of signal photons as a function of the signal wavelength measured with $\lambda_p \approx 800$ nm and $p \sim 1$ mW

photon fields was analyzed using the Glan–Taylor prisms placed in the signal and idler channels.

With the short- and longpass filters installed and the Glan–Taylor prisms adjusted to transmit the respective orthogonal polarization modes, the signal–idler photon coincidence rate N_c measured as a function of the difference between the signal and idler photon detection times, τ, exhibits a sharp peak at $\tau = 0$ (Fig. 4a, b), indicating a strong correlation of photon pairs. The count rate of the single-photon avalanche detector in the signal channel, N_s, measured as a function of the pump power p is accurately fitted by quadratic function of the pump power (blue line in Fig. 4c). The idler photon count rate N_i (red line in Fig. 4c), on the other hand, is best fitted with a polynomial $a_1p^2 + a_2p + a_3$, indicating a residual Raman noise in the idler channel. With the efficiency of photon detection provided by our detection scheme estimated as ~0.5%, the net signal–idler photon coincidence rate of $N_c \sim 10^5$ Hz is achieved near the central, $\tau = 0$ peak in Fig. 4a, b for $p \sim 1$ mW. This net signal–idler coincidence rate also closely follows the p^2 scaling within a broad range of p (Fig. 4d).

The coincidence-to-accidental ratio, defined as [21] $C/A = N_c f_p / (N_s N_i)$, is a decreasing function of the pump power p (black circles in Fig. 4c), in full agreement with a standard theory of photon-pair generation in FWM. With the pump power kept at a level of $p \approx 0.125$ mW, C/A ratios as high as 250: 1 are achieved in our photon-pair generation scheme (Fig. 4c). As p is reduced below this level, the signal and photon count rates become comparable with dark count rates in both detectors, lowering the C/A ratio. As earlier milestones, Morris et al. [22] report $C/A \approx 80$ with $N_c \sim 10^3$ Hz or $C/A \approx 19$ with $N_c \approx 6 \times 10^6$ Hz, Slater et al. [23] have demonstrated $C/A \approx 18$ with $N_c \approx 1.4 \times 10^5$ Hz, Ling et al. [24] have achieved $C/A \approx 900$ with $N_c \approx 2 \times 10^3$ Hz or $C/A \approx 10$ with $N_c \sim 10^6$ Hz.

With the short- and longpass filters in the signal and idler channels removed, the signal and idler count rates increase by more than two orders of magnitude, while the C/A becomes unity with a very high accuracy. This result is fully consistent with spectral measurements presented in Fig. 3a, clearly indicating that the Raman-scattered photons play an overwhelmingly dominant role in the signal and idler count rates. These findings also confirm that our experimental approach, based on correlated photon generation through FWM with high-Ω phase matching combined with appropriate spectral and polarization filtering, allows the background count rates related to uncorrelated Raman photon pairs to be reduced by more than two orders of magnitude. With the Glan–Taylor prisms installed in the signal and idler channels in such a way as to transmit the respective polarization modes of the signal and idler fields, these prisms help reduce the Raman background in the signal and especially in the idler photon count rates, but have almost no effect, apart from the inevitable Fresnel losses, on the coincidence count rate. As can be seen from Fig. 1d, e, the FWM sideband frequency Ω can be further increased by decreasing the pump wavelength, thus leading to an even lower level of the Raman noise and, hence, higher C/A ratios. However, this

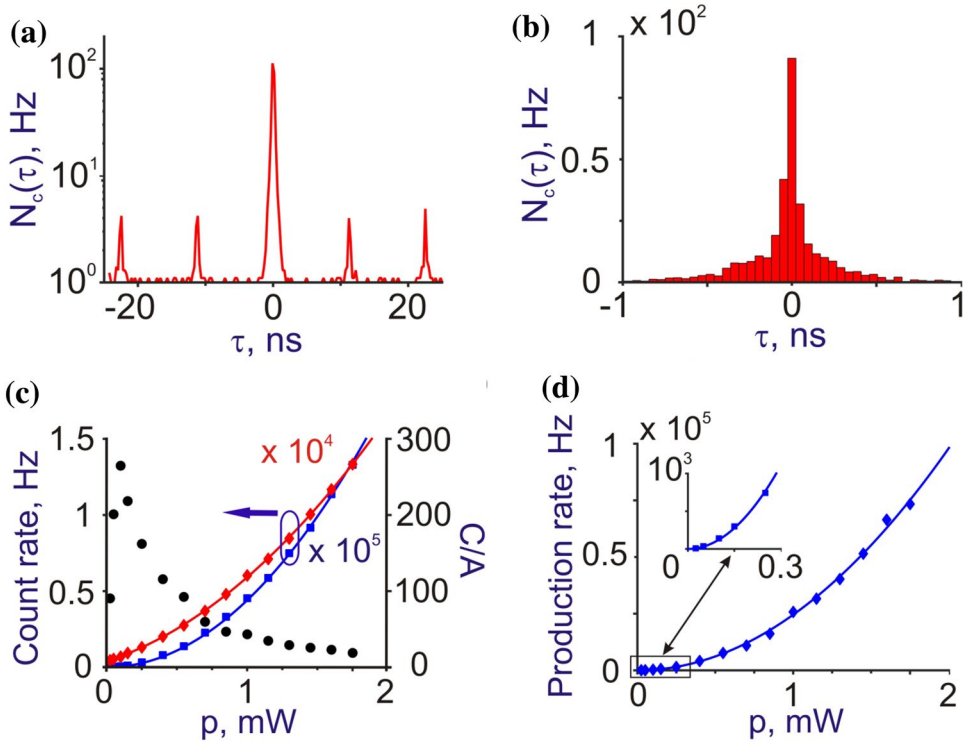

Fig. 4 **a** Time-correlated signal–idler photon coincidence rate N_c as a function of the difference between the signal and idler photon detection times, τ, for $p \approx 0.4$ mW. **b** The close-up of the central peak of the $N_c(\tau)$ trace. **c** The signal (blue) and idler (red) photon count rates along with the coincidence-to-accidental ratio C/A (black circles) as functions of p for $\varphi = \pi/4$. **d** The net signal–idler photon coincidence rate as a function of p for $\varphi = \pi/4$

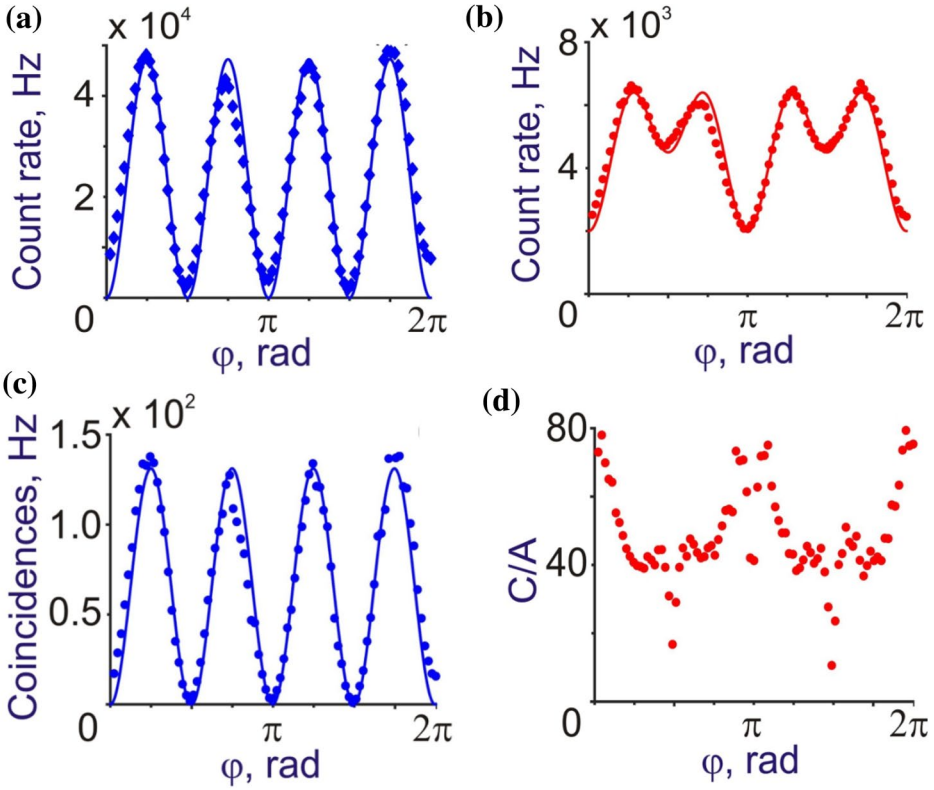

Fig. 5 **a–c** The signal (**a**), idler (**b**), and coincidence (**c**) count rates measured as functions of the angle ϕ for p ≈ 1 mW and $\lambda_p \approx$ 800 nm. The solid line is the $4a[\sin^2(\varphi)\cos^2(\varphi)] + b[\sin^2(\varphi)] + c[\text{co}$ fit with $b/a = c/a = 0$ (**a, c**) and $b/a = 3/2$ and $c/a = 2/3$ (**b**). **d** The *C/A* ratio measured as a function of ϕ

is achieved at the expense of a lower efficiency of FWM, and, as a consequence, a lower brightness of photon-pair generation.

Both the signal and idler photon count rates, as well as the coincidence count rate are highly sensitive to the polarization of the input pump field, displaying well-resolved oscillations as functions of ϕ (Fig. 5a–c). This behavior of the signal and idler photon count rates is fully consistent with the overall physical picture of correlated photon pair generation through the $\chi^{(3)}_{1212}$ FWM process. With the pump fields polarized along the fast and slow axes of the fiber given by $E_p^f = E_p\cos\varphi$ and $E_p^s = E_p\sin\varphi$, respectively, the signal, idler and coincidence count rates in pure $\chi^{(3)}_{1212}$ FWM should all follow the $\sin^2(\varphi)\cos^2(\varphi)$ behavior. Indeed, the signal count rate and the coincidence rate measured as functions of φ in our experiments are accurately fitted by the $\sin^2(\varphi)\cos^2(\varphi)$ dependence (Fig. 5a, c). The angular dependence of the idler count rate, on the other hand, indicates a measurable Raman-photon background in idler photon counts. The φ dependence of the idler signal count rate can be fitted with a $4a[\sin^2(\varphi)\cos^2(\varphi)] + b[\sin^2(\varphi)] + c[\cos^2(\varphi)]$ function (Fig. 5b). The first term of this fit represents correlated photons, while the second and third terms correspond to the Raman-scattered photons in orthogonal polarization modes. The behavior of the C/A ratio measured as function of φ (Fig. 5d) also displays clear signatures of the Raman noise in idler counts. With $\varphi = 0, \pi, 2\pi, \ldots$, this ratio peaks as the Raman noise is strongly suppressed by the analyzer. With $= \pi/2, 3\pi/2, \ldots$, on the other hand, C/A drastically decreases, as much of the Raman noise is transmitted through the analyzer.

To summarize, the FWM process with cross-polarized pump and cross-polarized sidebands, related to the $\chi^{(3)}_{1212}$ component of the cubic susceptibility tensor, provides a powerful resource of quantum entanglement, enabling creation of efficient fiber-optic sources of entangled photon pairs. Our experiments demonstrate that high-quality cross-polarized photon pairs can be generated in this new FWM geometry by coupling the laser pump into orthogonal polarization modes of a highly birefringent, highly nonlinear, anomalously dispersive PCF. With the pump wavelength chosen deeply within the anomalous dispersion region of the fiber, the frequency offset of the photon pairs relative to the pump frequency is adjusted to exceed 45 THz for an efficient suppression of the Raman noise, yielding photon pairs with the coincidence-to-accidental ratio as high as 250: 1.

Acknowledgements This research has been supported by the Government of Russian Federation (project no. 14.Z50.31.0040, Feb. 17, 2017).

References

1. J.E. Sharping, J. Chen, X. Li, P. Kumar, R.S. Windeler, Opt. Express **12**, 3086 (2004)
2. J.G. Rarity, J. Fulconis, J. Duligall, W.J. Wadsworth, P.StJ. Russell, Opt. Express **13**, 534 (2005)
3. J. Fulconis, O. Alibart, W.J. Wadsworth, P.StJ. Russell, J.G. Rarity, Opt. Express **13**, 7572 (2005)
4. J. Fulconis, O. Alibart, J.L. O'Brien, W.J. Wadsworth, J.G. Rarity, Phys. Rev. Lett. **99**, 120501 (2007)
5. O. Cohen, J.S. Lundeen, B.J. Smith, G. Puentes, P.J. Mosley, I.A. Walmsley, Phys. Rev. Lett. **102**, 123603 (2009)
6. M. Medic, J.B. Altepeter, M.A. Hall, M. Patel, P. Kumar, Opt. Lett. **35**, 802 (2010)
7. K. Garay-Palmett, H.J. McGuinness, O. Cohen, J.S. Lundeen, R. Rangel-Rojo, A.B. U'Ren, M.G. Raymer, C.J. McKinstrie, S. Radic, I.A. Walmsley, Opt. Express **15**, 14870 (2007)
8. P. Russell, Science **299**, 358 (2003)
9. N.L. Petrov, A.A. Voronin, A.B. Fedotov, A.M. Zheltikov, Appl. Phys. Lett. **110**, 181108 (2017)
10. X. Li, P.L. Voss, J.E. Sharping, P. Kumar, Phys. Rev. Lett. **94**, 053601 (2005)
11. C.J. McKinstrie, S.J. van Enk, M.G. Raymer, S. Radic, Opt. Express **16**, 2720 (2008)
12. C.J. McKinstrie, J.D. Harvey, S. Radic, M.G. Raymer, Opt. Express **13**, 9131 (2005)
13. M. Halder, J. Fulconis, B. Cemlyn, A. Clark, C. Xiong, W.J. Wadsworth, J.G. Rarity, Opt. Express **17**, 4670 (2009)
14. J. Fan, A. Migdall, Opt. Express **13**, 5777 (2005)
15. B.J. Smith, P. Mahou, O. Cohen, J.S. Lundeen, I.A. Walmsley, Opt. Express **17**, 23589 (2009)
16. J. Fan, A. Migdall, L.J. Wang, Opt. Lett. **30**, 3368 (2005)
17. Q. Lin, F. Yaman, G.P. Agrawal, Phys. Rev. A **75**, 023803 (2007)
18. G.P. Agrawal, *Nonlinear Fiber Optics*, 4th ed. (New York, Academic, 2007)
19. A.M. Zheltikov, Opt. Commun. **252**, 78 (2005)
20. A.M. Zheltikov, Sci. Rep. **7**, 46115 (2017)
21. S.V. A.Migdall, J. Polyakov, Fan, J.C. Bienfang, *Single-Photon Generation and Detection: Physics and Applications* (Amsterdam, Academic, 2013)
22. O.J. Morris, R.J.A. Francis-Jones, K.G. Wilcox, A.C. Tropper, P.J. Mosley, Opt. Commun. **327**, 39 (2014)
23. J.A. Slater, J.-S. Corbeil, S. Virally, F. Bussières, A. Kudlinski, G. Bouwmans, S. Lacroix, N. Godbout, W. Tittel, Opt. Lett. **35**, 499 (2010)
24. A. Ling, J. Chen, J. Fan, A. Migdall, Opt. Express **17**, 21302 (2009)